

NEW ACCURATE MEASUREMENT OF $^{36}\text{ArH}^+$ AND $^{38}\text{ArH}^+$ RO-VIBRATIONAL TRANSITIONS BY HIGH RESOLUTION IR ABSORPTION SPECTROSCOPY

M. CUETO¹, J. CERNICHARO², M. J. BARLOW³, B. M. SWINYARD^{3,4}, V. J. HERRERO¹, I. TANARRO¹, AND J. L. DOMÉNECH¹

¹ Molecular Physics Department, Instituto de Estructura de la Materia (IEM-CSIC), Serrano 123, E-28006 Madrid, Spain; jl.domenech@csic.es

² Department of Astrophysics, CAB. INTA-CSIC. Crta Torrejón-Ajalvir Km 4, E-28850 Torrejón de Ardoz, Madrid, Spain

³ Department of Physics and Astronomy, University College London. Gower Street, London WC1E 6BT, UK

⁴ Space Science and Technology Department, Rutherford Appleton Laboratory, Didcot OX11 0QX, UK

Received 2014 January 16; accepted 2014 January 24; published 2014 February 13

ABSTRACT

The protonated argon ion, $^{36}\text{ArH}^+$, was recently identified in the Crab Nebula from *Herschel* spectra. Given the atmospheric opacity at the frequency of its $J = 1-0$ and $J = 2-1$ rotational transitions (617.5 and 1234.6 GHz, respectively), and the current lack of appropriate space observatories after the recent end of the *Herschel* mission, future studies on this molecule will rely on mid-infrared observations. We report on accurate wavenumber measurements of $^{36}\text{ArH}^+$ and $^{38}\text{ArH}^+$ rotation-vibration transitions in the $v = 1-0$ band in the range 4.1–3.7 μm (2450–2715 cm^{-1}). The wavenumbers of the $R(0)$ transitions of the $v = 1-0$ band are 2612.50135 ± 0.00033 and 2610.70177 ± 0.00042 cm^{-1} ($\pm 3\sigma$) for $^{36}\text{ArH}^+$ and $^{38}\text{ArH}^+$, respectively. The calculated opacity for a gas thermalized at a temperature of 100 K and with a linewidth of 1 km s^{-1} of the $R(0)$ line is $1.6 \times 10^{-15} \times N(^{36}\text{ArH}^+)$. For column densities of $^{36}\text{ArH}^+$ larger than 1×10^{13} cm^{-2} , significant absorption by the $R(0)$ line can be expected against bright mid-IR sources.

Key words: ISM: molecules – methods: laboratory: molecular – molecular data – techniques: spectroscopic

Online-only material: machine-readable table

1. INTRODUCTION

Molecular complexes containing noble gas atoms have long been searched for in space without success, using space platforms and ground-based observatories. The presence of HeH^+ in the atmospheres of bright stars was suggested by Stecher & Milligan (1961, 1962) to explain the differences between observations and stellar models in the ultraviolet (see also Norton 1964; Harris et al. 2004). The role of HeH^+ in the chemistry of the early universe has also been a subject of debate (see, e.g., Lepp & Shull 1984; Galli & Palla 1998; Bovino et al. 2011) and searches have been conducted to try to detect this molecular ion in high redshift objects (Zinchenko et al. 2011), albeit unsuccessfully.

Barlow et al. (2013) have recently reported the serendipitous detection of $^{36}\text{ArH}^+$ in the emission spectra of the Crab Nebula during a search for CO lines. In our planet, the most abundant Ar isotope is ^{40}Ar , produced from the disintegration of ^{40}K through electron capture or positron emission, and from beta decay of ^{40}Ca . However, in space the most abundant isotope is ^{36}Ar , produced by alpha processes during stellar nucleosynthesis. The abundances on Earth of ^{38}Ar , ^{36}Ar , and ^{40}Ar are 0.063%, 0.337%, and 99.600%, respectively. However, in the Sun, 84.6% of argon is ^{36}Ar (Lodders 2008) and in giant planets $^{36}\text{Ar}/^{40}\text{Ar}$ is 8600 (Cameron 1973). As a consequence of the high abundance of the heavy ^{40}Ar on Earth, most laboratory studies of ArH^+ have focused on $^{40}\text{ArH}^+$ and little information is available for $^{36}\text{ArH}^+$, and even less for $^{38}\text{ArH}^+$. Barlow et al. (2013) discovered $^{36}\text{ArH}^+$ using the submillimeter Fourier Transform Spectrometer (SPIRE; Griffin et al. 2010) on board the *Herschel* satellite (Pilbratt et al. 2010). The frequency of the $J = 1-0$ line of $^{36}\text{ArH}^+$ is 617.5 GHz, for which the atmospheric transmission is rather poor even for a site as good as that of ALMA. The $J = 2-1$ line occurs at 1.235 THz and its observation from the ground is impossible due to telluric absorption. Hence,

space platforms are best for the observation of the pure rotational lines of this molecule in space. As an alternative, after the end of the *Herschel* mission, ro-vibrational transitions of ArH^+ isotopologues could be observed in absorption against bright background mid-infrared sources, such as the galactic center.

There are a number of high resolution spectroscopic studies on all isotopologues of this ion (i.e., with ^{40}Ar , ^{36}Ar , ^{38}Ar , H, and D) in the literature, both in the infrared and in the submillimeter wave region. The work by Odashima et al. (1999) is the last published addition of laboratory frequency data, and references to previous work can be found there. Remarkably, for $^{36}\text{ArH}^+$ and $^{38}\text{ArH}^+$, the only direct measurements are six and two, ro-vibrational lines, respectively, by Filgueira & Blom (1988) and by Haese and Oka (unpublished results, quoted by Johns 1984), using the natural isotopic abundance of ^{36}Ar and ^{38}Ar in both cases.

In this Letter we report on the accurate laboratory measurement of 19 lines of the $v = 1-0$ band of $^{36}\text{ArH}^+$ and $^{38}\text{ArH}^+$ which have been used to fit all available laboratory data of all ArH^+ isotopologues. The mass-independent Dunham coefficients have been considerably improved. Accurate wavenumbers are provided to help in the search and detection of $^{36}\text{ArH}^+$ and other isotopologues of ArH^+ in space in the mid-infrared.

2. EXPERIMENTAL DETAILS

The apparatus used in this experiment has been reported earlier (Doménech et al. 2013; Tanarro et al. 1994), and has been recently used to confirm the identification of NH_3D^+ in space (Cernicharo et al. 2013). It is based on an IR difference-frequency laser spectrometer, a hollow cathode discharge reactor, and a double modulation technique with phase-sensitive detection (Domingo et al. 1994).

Briefly, frequency-tunable IR radiation is generated by mixing the output of an Ar^+ laser with that of a tunable ring dye laser in a LiNbO_3 crystal contained in a temperature-controlled

oven. The wavelength coverage is $\sim 2.2\text{--}4.2\ \mu\text{m}$, with $\sim 3\ \text{MHz}$ linewidth and $\sim 5\ \mu\text{W}$ power. The Ar^+ laser is locked to the $^{127}\text{I}_2$ a_3 hyperfine component of the $P(13)$ $43\text{--}0$ transition, known to $\sim 0.1\ \text{MHz}$ accuracy (Quinn 2003). The laser frequency has a residual frequency jitter $< 1\ \text{MHz}$ and similar long-term stability. The tunable single mode ring dye laser is also frequency stabilized, with commercial stabilization electronics (residual jitter $< 3\ \text{MHz}$). Its wavelength is measured with a high accuracy ($10\ \text{MHz}$ (3σ)) commercial wavemeter (High Finesse WSU10), calibrated with the stabilized Ar^+ laser. The wavemeter accuracy limits that of the IR frequency scale.

The discharge is modulated at $3.09\ \text{kHz}$ through an audio amplifier, a step-up transformer, and a $940\ \Omega$ ballast resistor. Typical discharge conditions are $250\ \text{V}$ rms between electrodes and $375\ \text{mA}$. The IR beam is amplitude modulated at $23.19\ \text{kHz}$ with an electro-optic modulator and a polarizer placed in the path of the Ar^+ laser beam. The IR beam is split before the absorption cell so that one part is directed to an InSb detector and is used for noise reduction and the other one goes through the multipass cell 32 times ($22.4\ \text{m}$ path length) and is then detected by another InSb detector. To improve the sensitivity for the $^{36}\text{ArH}^+$ and $^{38}\text{ArH}^+$ isotopologues, an autobalanced transimpedance amplifier (ATA) based on the design of Lindsay et al. (2001) has been built and added to the set-up. The ATA output is fed to a dual-phase lock-in amplifier synchronized at the sum frequency of both modulation signals ($26.28\ \text{kHz}$). The detection time constant is $30\ \text{ms}$ with $12\ \text{dB oct}^{-1}$ roll off and scans were made at a rate of $0.005\ \text{cm}^{-1}\ \text{s}^{-1}$ (about 30 time constants per line width) to avoid line-shape distortion effects. The ATA halves the floor noise level, reducing by a factor of four the acquisition time necessary to attain a given signal-to-noise ratio (S/N). For $^{36}\text{ArH}^+$ and $^{38}\text{ArH}^+$, between 100 and 800 scans were averaged to obtain S/Ns between 12 and 50. The width of the scans, $0.05\ \text{cm}^{-1}$ (about 8 line widths FWHM), keeps the recording time to a minimum and allows a good estimation of the baseline. A symmetric triangle wave is programmed to control the scans, so the lines are recorded both with increasing and decreasing wavenumber scale. The full data set of frequency and intensity values is frequency-binned and averaged in a $0.0005\ \text{cm}^{-1}$ grid. The wavemeter is recalibrated with the frequency-stabilized Ar^+ laser after every 50 scans.

The reactor is pumped down to 10^{-3} mbar. A continuous flow ($\sim 30\ \text{mg minute}^{-1}$) of Ar with natural isotopic composition (Air Liquide, 99.9995% purity) at $0.4\ \text{mbar}$ pressure is used to generate the ArH^+ ions in the discharge. Attempts to increase the ArH^+ IR absorption signal by adding H_2 were unsuccessful, indicating that the hydrogen concentration necessary to produce maximum ArH^+ absorption signals is very small and is thought to proceed from the tiny amount of residual water. ArH^+ in glow discharge plasmas is known to be produced mainly through the reactions $\text{H}_2^+ + \text{Ar} \rightarrow \text{ArH}^+ + \text{H}$ ($k = 2.1 \times 10^{-9}\ \text{cm}^3\ \text{s}^{-1}$) and $\text{Ar}^+ + \text{H}_2 \rightarrow \text{ArH}^+ + \text{H}$ ($k = 8.7 \times 10^{-10}\ \text{cm}^3\ \text{s}^{-1}$; Anicich 1993) and to be destroyed mainly through the reaction $\text{ArH}^+ + \text{H}_2 \rightarrow \text{H}_3^+ + \text{Ar}$ ($k = 6.3 \times 10^{-10}\ \text{cm}^3\ \text{s}^{-1}$). Recent kinetic studies on Ar/ H_2 discharges with relatively large proportions of H_2 show appreciable amounts of ArH^+ (Méndez et al. 2010; Sode et al. 2013). Nevertheless, previous spectroscopic studies of ArH^+ show that a fairly small proportion of H_2 (ranging from ~ 0.1 to $\sim 10\%$ in the studies of Haese et al. 1983, Johns 1984, Laughlin et al. 1987, Brown et al. 1988 and Filgueira & Blom 1988) or no supply at all of H_2 (Brault & Davis 1982) to the discharge gives larger ArH^+ signals.

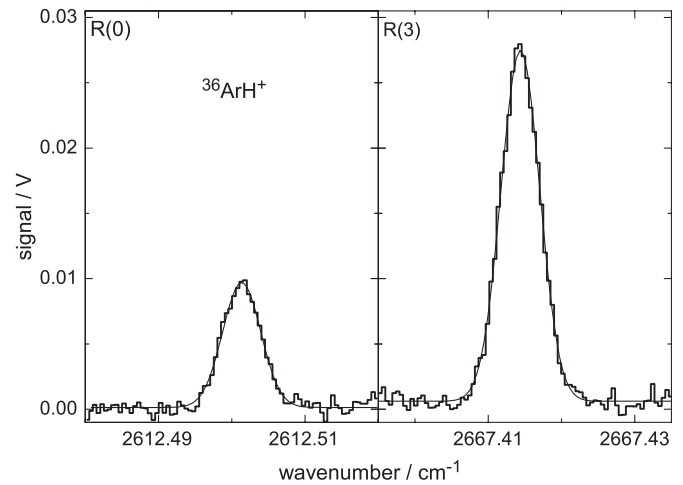


Figure 1. $R(0)$ and $R(3)$ lines of the $^{36}\text{ArH}^+$ isotopologue with their Gaussian fits.

3. RESULTS AND DISCUSSION

We have chosen the $R(6)$ line of the $v = 1\text{--}0$ band of $^{40}\text{ArH}^+$ at $2711.4029\ \text{cm}^{-1}$ as a reference to optimize the operating conditions and check the day-to-day repeatability of the experiment. We can observe this line in a single scan with S/N of 1100. Its Doppler FWHM is $0.0059\text{--}0.0061\ \text{cm}^{-1}$, corresponding to a kinetic temperature of $\sim 380\text{--}400\ \text{K}$. From the relative line intensities of $R(6)$ observed in the $v = 1\text{--}0$ and $v = 2\text{--}1$ bands, the estimated vibrational temperature is $\sim 580\ \text{K}$.

We estimate the density of ArH^+ in the discharge to be $\sim 4 \times 10^{10}\ \text{cm}^{-3}$, derived from the transition dipole moments and Herman–Wallis factors for $^{40}\text{ArH}^+$ in various vibrational bands given by Picqué et al. (2000), the estimated vibrational and rotational (kinetic) temperatures, and the observed peak absorption (typically ~ 0.035) in the $R(6)$ $v = 1\text{--}0$ line of $^{40}\text{ArH}^+$. This is a rough estimate, since ion signals exhibit day-to-day variations of up to 40%, depending on the discharge behavior. Nonetheless, this value is close to the total electron densities measured in this type of plasma (Méndez et al. 2010), suggesting that ArH^+ is a dominant ion in our discharge.

We have measured 14 lines of $^{36}\text{ArH}^+$ in the $v = 1\text{--}0$ band ($P(6)$ to $R(7)$) ranging from 2458.4 to $2729.3\ \text{cm}^{-1}$. We have scanned $0.05\ \text{cm}^{-1}$ wide regions, centered on the frequencies calculated from the Dunham parameters of Johns (1984). The predictions are rather accurate, and the lines were found within $\pm 2.2 \times 10^{-4}\ \text{cm}^{-1}$ of their expected value. Typically, 200 scans were averaged. The line center position has been derived from a least-squares fit of each line to a Gaussian function. As an example, the $R(0)$ and $R(3)$ lines are shown together with their Gaussian fits in Figure 1. The uncertainty in the line positions is estimated as the quadratic sum of the standard error of the line center derived from the fit plus the manufacture-stated accuracy of the wavemeter, i.e., $3.3\ \text{MHz}$ (1σ). The observed line centers and their estimated uncertainties (1σ) are given in Table 1.

These new data for $^{36}\text{ArH}^+$ have been fitted to the frequencies derived from the energy levels calculated with a simple Hamiltonian for a vibrating rotor (Herzberg 1989)

$$E(v, J) = \nu_0 + B_v J(J+1) - D_v [J(J+1)]^2 + H_v [J(J+1)]^3 + \dots \quad (1)$$

Despite the relatively low number of measurements, the quality of the data allows us to determine, with statistical

Table 1
Observed Line Centers, Their Estimated 1σ Uncertainties,
and Spectroscopic Constants of $^{36}\text{ArH}^+$

Isotopologue	Line	ν_{obs} (cm^{-1})	σ^a	$(O - C)^b$	Constant ^c (cm^{-1})
$^{36}\text{ArH}^+$	$P(6)$	2458.36336	11.4	0.3	B_0 10.30044364(778)
	$P(5)$	2482.47613	11.3	-5.5	D_0 $6.21374(154) \times 10^{-4}$
	$P(4)$	2505.91727	10.5	7.7	ν_1 2592.651339(42)
	$P(3)$	2528.67068	11.6	3.8	B_1 9.92620133(616)
	$P(2)$	2550.72091	11.8	-8.9	D_1 $6.127689(908) \times 10^{-4}$
	$P(1)$	2572.05291	13.2	-2.8	
	$R(0)$	2612.50135	11.3	5.9	
	$R(1)$	2631.58798	11.1	-10.6	
	$R(2)$	2649.89731	10.3	8.6	
	$R(3)$	2667.41441	10.4	-0.3	
	$R(4)$	2684.12561	11.9	4.6	
	$R(5)$	2700.01671	11.4	-8.8	
	$R(6)$	2715.07445	11.3	0.9	
	$R(7)$	2729.28504	11.0	2.0	
$^{38}\text{ArH}^+$	$R(0)$	2610.70177	13.9		
	$R(1)$	2629.76268	11.2		
	$R(2)$	2648.04731	13.4		
	$R(3)$	2665.54197	14.9		
	$R(4)$	2682.23225	13.9		

Notes.

^a σ = estimated uncertainty/ 10^{-5} cm^{-1} .

^b $(O - C) = (\nu_{\text{obs}} - \nu_{\text{calc}}) / 10^{-5} \text{ cm}^{-1}$.

^c Numbers in parentheses are one standard deviation in units of the last quoted digit, as derived from the fit.

significance, five independent parameters (up to the D centrifugal distortion constants), with an uncertainty-weighted standard deviation $\sigma_w = 0.61$. Recall that σ_w is close to unity for an adequate model and reasonable estimates of the experimental uncertainties. The low σ_w value reflects an internal coherence of the frequency better than the uncertainty, as is reasonable to expect. As a further check, with the parameters determined in this fit, we calculate the frequency of the 1–0 rotational transition of $^{36}\text{ArH}^+$ at $617524.4 \pm 1.2 \text{ MHz}$ ($\pm 3\sigma$), which compares very well with the frequency predicted by the Cologne database (Müller et al. 2005) of $617525.23 \pm 0.45 \text{ MHz}$ ($\pm 3\sigma$). As noted in Section 1, prior to this work, only six direct measurements of ro-vibrational frequencies of $^{36}\text{ArH}^+$ were available. The accuracy of the previous values, estimated by their authors, was $\sim 0.001 \text{ cm}^{-1}$. No measurements of $R(0)$ have been reported previously.

As for $^{38}\text{ArH}^+$, we have recorded five previously unreported lines, $R(0)$ to $R(4)$, in the $v = 1-0$ band. Given their weakness, it was necessary to average up to 800 scans for some of them. Since the efficiency of the difference frequency mixing process decreases with the IR frequency, and phonon absorption from LiNbO_3 starts to become significant at lower frequencies, the IR power available for lines in the P branch was not sufficient to record them in a reasonable amount of time. The wavenumbers determined in this work and their uncertainties are shown in Table 1. As an example, the $R(0)$ and $R(2)$ lines are shown in Figure 2, together with their Gaussian fits. Filgueira & Blom (1988) reported the observation of the $P(3)$ and $P(4)$ lines, with $\sim 0.001 \text{ cm}^{-1}$ accuracy, and, similar to $^{36}\text{ArH}^+$, no measurements of $R(0)$ have been reported previously. Given the reduced number of lines in this case, we have not attempted an independent fit of this isotopologue.

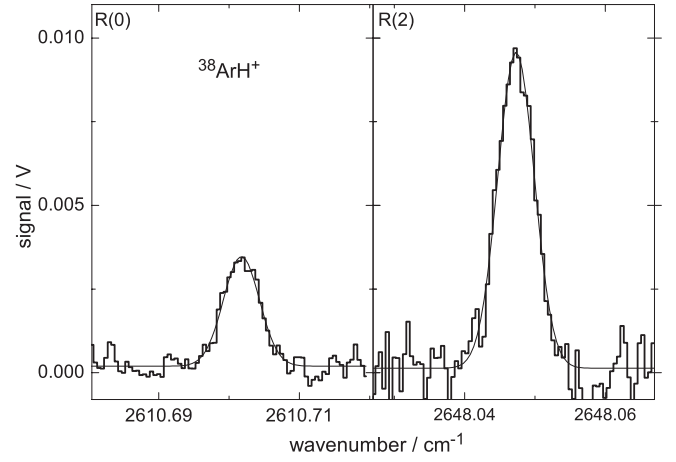


Figure 2. $R(0)$ and $R(2)$ lines of the $^{38}\text{ArH}^+$ isotopologue with their Gaussian fits.

These new measurements, together with all previous infrared and millimeter-wave data found in the literature for all isotopologues of ArH^+ (i.e., those including ^{40}Ar , ^{36}Ar , ^{38}Ar , H, and D) have been combined in a global fit to a mass-independent Dunham’s series expansion for a diatomic molecule in a $^1\Sigma$ state (Watson 1980)

$$\begin{aligned}
 E(v, J) = & \sum_{kl} \mu^{-(k/2+l)} U_{kl} \\
 & \times (1 + m_e \Delta_{kl}^{\text{Ar}} / M_{\text{Ar}} + m_e \Delta_{kl}^{\text{H}} / M_{\text{H}}) \\
 & \times \left(v + \frac{1}{2} \right)^k [J(J+1)]^l, \quad (2)
 \end{aligned}$$

where U_{kl} and Δ_{kl}^i are mass-independent coefficients (Δ_{kl}^i are the Born–Oppenheimer approximation breakdown, or BOB, terms), M_{Ar} and M_{H} the atomic masses of the corresponding isotope (Coursey et al. 2010), m_e the electron mass, and μ is a charge-modified reduced mass, defined for ArH^+ as

$$\mu = \frac{M_{\text{Ar}} M_{\text{H}}}{M_{\text{Ar}} + M_{\text{H}} - m_e}. \quad (3)$$

In the fitting process it became evident that a significantly better global fit is obtained if, in the calculation of μ , we use $(M_{\text{Ar}} - m_e)$ in the numerator instead of the Ar atomic mass M_{Ar} . In this case, $\sigma_w = 0.72$, while that obtained using Equation (3) is $\sigma_w = 0.86$. Using $(M_{\text{Ar}} - m_e)$ amounts to centering all the positive charge of the ion on the Ar nucleus. Similar improvements in a Born–Oppenheimer potential fit using different expressions of μ were observed in HeH^+ by Coxon & Hajigeorgiou (1999), although in that case the best fit was obtained if half the electron mass was subtracted from that of each atom. Furthermore, an ab-initio study of noble gas hydride molecule ions (Schutte 2002) shows a progressive displacement of the positive charge of the ion from the H nucleus to the noble gas nucleus, at the equilibrium distance, in going from HeH^+ to KrH^+ . Therefore, we deemed it advisable to carry out four fits using different calculations for the reduced mass: using Watson’s (1980) expression; equally splitting the charge between both nuclei; completely ignoring the electron mass (i.e., treating the molecule as neutral), and assigning all the charge to the Ar nucleus (as described above). The σ_w are 0.86, 0.76, 0.72, and 0.72, respectively. In order to better reproduce the set

of existing observations, we have chosen the latter as our best fit, regardless of the possible implications on the adequacy of Equation (3) to calculate the charge-corrected reduced mass of light ions, or on the effect of μ on the physical meaning of the Dunham parameters thus derived.

The fit has been carried out using a linear least-squares fitting program coupled to the MADEX code (Cernicharo 2012), which allows us to predict the frequencies of the pure rotational and ro-vibrational lines of all the isotopologues of ArH⁺ from the parameters provided by the fitting routine. The fit contains 367 experimental frequencies, weighted by the square of their estimated reciprocal uncertainty. The results are shown in Table 2 together with the parameters obtained by fitting all the previous data prior to this work. The parameters with no uncertainty have been fixed to the values derived from the fitted parameters and the Dunham relations to U_{k0} , U_{kl} as provided by the code ACET of the Computer Physics Communications library written by Ogilvie (1983). Including the BOB term Δ_{01}^{Ar} does not improve the quality of the fit. In both fits, $(M_{\text{Ar}} - m_e)$ has been used in the numerator of Equation (3) to calculate μ . Summarizing the results, before the inclusion of the new data reported in this Letter, the standard deviation of the fit was 52.5 MHz, which decreases to 50.7 MHz when our new wavenumbers are included. The relatively small change in the standard deviation is due to the reduced number of new accurate data. Nevertheless, significant improvements are obtained in the U_{10} , U_{12} and Δ_{10}^{Ar} parameters, whose standard deviations decrease by factors of 1.8, 1.4, and 5.6, respectively, when the present wavenumbers are taken into account. The change in the rest of the parameters is marginal, accompanied by a less significant decrease of their standard deviations due to the large number of pure rotational lines measured with high accuracy for $^{40}\text{ArH}^+$ and $^{40}\text{ArD}^+$. The Δ_{01}^{Ar} BOB parameter is poorly determined even with those data for the pure rotational lines (see Odashima et al. 1999). Using U_{kl} and Δ_{kl}^i from Table 2 we can predict the frequencies of the pure rotational lines of all isotopologues with high accuracy. The $J = 1-0$ transition is predicted at 617525.134 ± 0.100 , 616648.720 ± 0.100 , and 615858.136 ± 0.100 MHz for $^{36}\text{ArH}^+$, $^{38}\text{ArH}^+$, and $^{40}\text{ArH}^+$, respectively. The predicted wavenumber of the $\nu = 1-0 R(0)$ line is $2612.50129 \pm (6 \times 10^{-5})$, $2610.70170 \pm (10 \times 10^{-5})$, and $2609.07719 \pm (20 \times 10^{-5}) \text{ cm}^{-1}$ for the same isotopologues. The quoted intervals are $\pm 3\sigma$ uncertainties. Table 3 contains all published observed frequencies of all isotopologues, as well as the values calculated from our fit.

The absorption coefficient of the $R(0)$ line can be computed from the transition dipole moment of the $\nu = 1-0$ transition derived by Picqué et al. (2000). We have used their value of $\mu_{1-0} = 0.297 \text{ D}$ based on the calculations of Rosmus (1979) for the permanent dipole moment of the ground vibrational state $\mu_0 = 2.2 \text{ D}$. They also provide a smaller value, $\mu_{1-0} = 0.194 \text{ D}$, based on the experimental determination of $\mu_0 = 1.42 \pm 0.6 \text{ D}$ by Laughlin et al. (1987). However, Laughlin et al. (1989) provided $\mu_0 = 3.0 \pm 0.6 \text{ D}$ after a refinement of their experiment, in better agreement with the value from Rosmus (1979). Both values are in good agreement with the calculations performed at a higher level of theory by Cheng et al. (2007) and by the analysis of the experimental potential curve by Molski (2001). Using $\mu_{1-0} = 0.297 \text{ D}$ we can derive $\tau(R(0)) = \alpha(T) \times N(\text{ArH}^+) / \Delta\nu$, where $N(\text{ArH}^+)$ is the column density of the molecule in cm^{-2} , $\Delta\nu$ is the linewidth in km s^{-1} , and $\alpha(T)$ is 9.5×10^{-15} , 1.6×10^{-15} , 3.2×10^{-16} , and 1.5×10^{-16} (in $\text{cm}^2 \text{ km s}^{-1}$) for $T = 10, 100, 500$, and 1000 K , respectively.

Table 2
Mass-independent Dunham Coefficients^a for ArH⁺

k	l	U_{kl} (This Work) ^b	U_{kl} (Previous Data) ^b
1	0	2688.29968(193)	2688.29896(345)
2	0	-60.56901(224)	-60.56869(227)
3	0	$4.9333(124) \times 10^{-01}$	$4.9320(123) \times 10^{-01}$
4	0	$-2.348(287) \times 10^{-03}$	$-2.332(284) \times 10^{-03}$
5	0	$-1.154(316) \times 10^{-04}$	$-1.162(313) \times 10^{-04}$
6	0	$-1.330(132) \times 10^{-05}$	$-1.329(131) \times 10^{-05}$
0	1	10.28307619(216)	10.28307575(219)
1	1	$-3.6901057(708) \times 10^{-01}$	$-3.6900543(738) \times 10^{-01}$
2	1	$2.92102(466) \times 10^{-03}$	$2.91688(478) \times 10^{-03}$
3	1	$9.25(165) \times 10^{-06}$	$1.028(168) \times 10^{-05}$
4	1	$-2.898(275) \times 10^{-06}$	$-3.022(279) \times 10^{-06}$
5	1	$-1.948(165) \times 10^{-07}$	$-1.896(167) \times 10^{-07}$
0	2	$-6.0181686(568) \times 10^{-04}$	$-6.0181497(568) \times 10^{-04}$
1	2	$7.89698(914) \times 10^{-06}$	$7.8769(126) \times 10^{-06}$
2	2	$1.469(381) \times 10^{-08}$	$2.146(410) \times 10^{-08}$
3	2	$-2.1555(349) \times 10^{-08}$	$-2.2871(351) \times 10^{-08}$
4	2	$2.887511467(0) \times 10^{-10}$	$4.188353696(0) \times 10^{-10}$
5	2	$-2.276400996(0) \times 10^{-11}$	$-2.531285219(0) \times 10^{-11}$
0	3	$1.54073(178) \times 10^{-08}$	$1.54146(187) \times 10^{-08}$
1	3	$-3.867(101) \times 10^{-10}$	$-3.745(120) \times 10^{-10}$
2	3	$-1.441(182) \times 10^{-11}$	$-1.732(218) \times 10^{-11}$
3	3	$2.367548148(0) \times 10^{-13}$	$6.839849573(0) \times 10^{-13}$
4	3	$-9.706972163(0) \times 10^{-13}$	$-1.029987077(0) \times 10^{-12}$
0	4	$-8.961(261) \times 10^{-13}$	$-9.148(293) \times 10^{-13}$
1	4	$1.074791089(0) \times 10^{-15}$	$2.300842563(0) \times 10^{-15}$
2	4	$-1.091227090(0) \times 10^{-14}$	$-1.135430007(0) \times 10^{-14}$
3	4	$-4.145809861(0) \times 10^{-16}$	$-4.269036526(0) \times 10^{-16}$
4	4	$3.101458722(0) \times 10^{-16}$	$3.303414639(0) \times 10^{-16}$
0	5	$2.203620896(0) \times 10^{-17}$	$2.202997632(0) \times 10^{-17}$
1	5	$-3.102378289(0) \times 10^{-18}$	$-3.367869218(0) \times 10^{-18}$
2	5	$1.657426695(0) \times 10^{-18}$	$1.894902940(0) \times 10^{-18}$
3	5	$-5.622789166(0) \times 10^{-19}$	$-5.889490755(0) \times 10^{-19}$
0	6	$-2.567213307(0) \times 10^{-21}$	$-2.537578808(0) \times 10^{-21}$
1	6	$-1.281992858(0) \times 10^{-21}$	$-1.307682397(0) \times 10^{-21}$
2	6	$-4.750748688(0) \times 10^{-22}$	$-5.139236544(0) \times 10^{-22}$
3	6	$2.274040168(0) \times 10^{-22}$	$2.408609282(0) \times 10^{-22}$
0	7	$-3.390838692(0) \times 10^{-26}$	$-3.984572007(0) \times 10^{-26}$
1	7	$1.797128568(0) \times 10^{-25}$	$1.996397008(0) \times 10^{-25}$
2	7	$-4.768691261(0) \times 10^{-26}$	$-4.646346036(0) \times 10^{-26}$

Notes.

^a The following BOB parameters (dimensionless) have also been fitted (this work [from the fit to the previous data]):

$$\begin{aligned} \Delta_{10}^{\text{Ar}} &= 1.824(145) \times 10^{-01} [2.017(813) \times 10^{-01}], \\ \Delta_{10}^{\text{H}} &= -3.3110(122) \times 10^{-01} [-3.3126(125) \times 10^{-01}], \\ \Delta_{20}^{\text{H}} &= 6.147(218) \times 10^{-01} [6.157(221) \times 10^{-01}], \\ \Delta_{01}^{\text{H}} &= 1.25816(439) \times 10^{-01} [1.25312(498) \times 10^{-01}], \\ \Delta_{11}^{\text{H}} &= 8.006(279) \times 10^{-01} [7.854(290) \times 10^{-01}], \\ \Delta_{02}^{\text{H}} &= 1.0098(384) [9.929(399) \times 10^{-01}]. \end{aligned}$$

^b Units are $\text{cm}^{-1} \text{ amu}^{k/2+l}$. Numbers in parentheses are 1σ uncertainties in units of the last quoted digit. An uncertainty of 0 means that the parameter has been fixed.

These values for $\alpha(T)$ have to be decreased by a factor of ~ 2.4 , or increased by a factor of ~ 1.9 , depending on whether the μ_0 value of Laughlin et al. (1987) or that of Laughlin et al. (1989) is assumed. The best conditions to detect the $R(0)$ lines are those of the diffuse interstellar medium lines of sight where the kinetic temperature could be below 100 K and no emission is expected from the $R(0)$ line. For the estimated column densities by Barlow et al. (2013) absorption in the $R(0)$ lines of a few percent could be expected. We note, however, that if the kinetic temperature of the gas in the Crab Nebula is above 1000 K, the $R(0)$ line, and others, could appear in emission. For column densities above

Table 3
Measured and Calculated Ro-vibrational Transitions of the Isotopologues of ArH⁺

Isotopologue	J_u	J_l	v_u	v_l	Units	ν_{obs}	σ_{obs}	ν_{cal}	σ_{cal}	$\nu_{\text{obs}} - \nu_{\text{cal}}$	Ref.
³⁶ ArH ⁺	7	6	1	0	cm ⁻¹	2715.0745	0.00011	2715.074333	0.000034	0.000117	1
³⁶ ArH ⁺	8	7	1	0	cm ⁻¹	2729.2850	0.00011	2729.285196	0.000041	-0.000156	1
³⁶ ArH ⁺	4	3	1	0	cm ⁻¹	2667.4140	0.00100	2667.414412	0.000021	-0.000412	2
³⁶ ArH ⁺	3	2	1	0	cm ⁻¹	2649.8960	0.00100	2649.897267	0.000022	-0.001267	2
³⁶ ArH ⁺	2	1	1	0	cm ⁻¹	2631.5890	0.00100	2631.588125	0.000024	0.000875	2
³⁶ ArH ⁺	1	2	1	0	cm ⁻¹	2550.7200	0.00100	2550.720959	0.000026	-0.000959	2
³⁶ ArH ⁺	2	3	1	0	cm ⁻¹	2528.6720	0.00100	2528.670669	0.000024	0.001331	2
³⁶ ArH ⁺	3	4	1	0	cm ⁻¹	2505.9180	0.00200	2505.917300	0.000022	0.000700	2
³⁶ ArD ⁺	1	0	0	0	MHz	319065.3790	0.06500	319065.389737	0.005378	-0.010737	3
³⁸ ArH ⁺	1	0	1	0	cm ⁻¹	2610.7018	0.00014	2610.701706	0.000036	0.000064	1
³⁸ ArH ⁺	2	1	1	0	cm ⁻¹	2629.7627	0.00011	2629.762543	0.000034	0.000137	1

Notes. Frequencies are in cm⁻¹ or in MHz as indicated. These units apply to all the elements of each row. Observed and predicted uncertainties (σ_{obs} and σ_{cal}) are 1 σ values. Transitions with $\sigma_{\text{obs}} = 0$ have been discarded from the fit due to a large $\nu_{\text{obs}} - \nu_{\text{cal}}$ value. (1) This work; (2) Filgueira & Blom 1988; (3) Bowman et al. 1983; (4) Brown et al. 1988; (5) Liu et al. 1987; (6) Brault & Davis 1982; (7) Johns 1984; (8) Laughlin et al. 1988; (9) Odashima et al. 1999.

(This table is available in its entirety in a machine-readable form in the online journal. A portion is shown here for guidance regarding its form and content.)

10¹³ cm⁻² the different isotopologues of ArH⁺ could be easily detected in cold dark clouds against bright sources through mid-IR observations.

4. CONCLUDING REMARKS

We have provided direct accurate wavenumber measurements of 19 vibration-rotation lines of ³⁶ArH⁺ and ³⁸ArH⁺ in natural isotopic abundance, measured with a difference frequency laser spectrometer and a hollow cathode discharge cell. Of those, only six had been reported before, and with much larger uncertainty. Furthermore, the new wavenumbers have improved the Dunham-type fit to all published rotation and vibration-rotation data for all isotopologues of this molecule, allowing more accurate predictions of other transitions for any of them. Notably, the measured wavenumbers of the $R(0)$ transitions of the $v = 1-0$ band are 2612.50135 ± 0.00033 and 2610.70177 ± 0.00042 cm⁻¹ ($\pm 3\sigma$) for ³⁶ArH⁺ and ³⁸ArH⁺ (predicted values of $2612.50129 \pm (6 \times 10^{-5})$ cm⁻¹ and $2610.70170 \pm (10 \times 10^{-5})$ cm⁻¹), respectively. These wavenumbers should help in future searches for absorptions of these molecules against bright sources.

The authors acknowledge the financial support from the Spanish MINECO through the Consolider Astromol project, grant CSD2009-00038. J.L.D. and M.C. acknowledge additional support through grant FIS2012-38175. V.H. and I.T. acknowledge additional support through grant FIS2010-16455. J.C. acknowledges additional support through grants AYA2009-07304 and AYA2012-32032. Our skillful technicians J. Rodríguez and M.A. Moreno are gratefully acknowledged.

REFERENCES

- Anicich, V. G. 1993, *JPCRD*, **22**, 1469
 Barlow, M. J., Swinyard, B. M., Owen, P. J., et al. 2013, *Sci*, **342**, 1343
 Bovino, S., Tacconi, M., Gianturco, F. A., & Galli, D. 2011, *A&A*, **529**, A140
 Bowman, W. C., Plummer, G. M., Herbst, E., & De Lucia, F. C. 1983, *JChPh*, **79**, 2093
 Brault, J. W., & Davis, S. P. 1982, *PhysS*, **25**, 268
 Brown, J. M., Jennings, D. A., Vanek, M., et al. 1988, *JMoSp*, **128**, 587
 Cameron, A. G. W. 1973, *SSRv*, **14**, 392
 Cernicharo, J. 2012, in *EAS Publications Series*, Vol. 58, ed. C. Stehl, C. Joblin, & L. d'Hendecourt (Cambridge: Cambridge Univ. Press), 251
 Cernicharo, J., Tercero, B., Fuente, A., et al. 2013, *ApJL*, **771**, L10
 Cheng, M., Brown, J. M., Rosmus, P., et al. 2007, *PhRvA*, **75**, 012502
 Coursey, J. S., Schwab, D. J., Tsai, J. J., & Dragoset, R. A. 2010, *Atomic Weights and Isotopic Compositions* (version 3.0; Gaithersburg, MD: National Institute of Standards and Technology), <http://physics.nist.gov/Comp>
 Coxon, J. A., & Hajigeorgiou, P. G. 1999, *JMoSp*, **193**, 306
 Doménech, J. L., Cueto, M., Herrero, V. J., et al. 2013, *ApJL*, **771**, L11
 Domingo, C., Tanarro, I., Herrero, V. J., et al. 1994, *Proc. SPIE*, **2124**, 227
 Filgueira, R. R., & Blom, C. E. 1988, *JMoSp*, **127**, 279
 Galli, D., & Palla, F. 1998, *A&A*, **335**, 403
 Griffin, M. J., Abergel, A., Abreu, A., et al. 2010, *A&A*, **518**, L3
 Haese, N., Pan, F.-S., & Oka, T. 1983, *PhRvL*, **50**, 1575
 Harris, G. J., Lynas-Gray, A. E., Miller, S., & Tennyson, J. 2004, *ApJL*, **617**, L143
 Herzberg, G. 1989, *Molecular Spectra and Molecular Structure*, Vol. 1, *Spectra of Diatomic Molecules* (Malabar, FL: Robert E. Krieger Publishing CO)
 Johns, J. W. C. 1984, *JMoSp*, **106**, 124
 Laughlin, K. B., Blake, G. A., Cohen, R. C., Hovde, D. C., & Saykally, R. J. 1987, *PhRvL*, **58**, 996
 Laughlin, K. B., Blake, G. A., Cohen, R. C., Hovde, D. C., & Saykally, R. J. 1988, *RSPTA*, **324**, 119
 Laughlin, K. B., Blake, G. A., Cohen, R. C., & Saykally, R. J. 1989, *JChPh*, **90**, 1358
 Lepp, S., & Shull, J. M. 1984, *ApJ*, **280**, 465
 Lindsay, C. M., Rade, R. M., Jr., & Oka, T. 2001, *JMoSp*, **210**, 51
 Liu, D.-J., Ho, W.-C., & Oka, T. 1987, *JChPh*, **87**, 2442
 Lodders, K. 2008, *ApJ*, **674**, 607
 Méndez, I., Tanarro, I., & Herrero, V. J. 2010, *PCCP*, **12**, 4239
 Molski, M. 2001, *CPL*, **342**, 293
 Müller, H. S. P., Schlöder, F., Stutzki, J., & Winnewisser, G. T. 2005, *JMoSt*, **742**, 215
 Norton, R. H. 1964, PhD thesis, California Institute of Technology
 Odashima, H., Kozato, A., Matsushima, F., Tsunekawa, S., & Takagi, K. 1999, *JMoSp*, **195**, 356
 Ogilvie, J. F. 1983, *CoPhC*, **30**, 101
 Picqué, N., Guelachvili, G., & Civiş, S. 2000, *JChPh*, **113**, 2134
 Pilbratt, G., Riedinger, J. R., Passvogel, T., et al. 2010, *A&A*, **518**, L1
 Quinn, T. J. 2003, *Metro*, **40**, 103
 Rosmus, P. 1979, *AcTc*, **51**, 359
 Schutte, C. J. H. 2002, *CPL*, **353**, 389
 Sode, M., Schwarz-Selinger, T., & Jacob, W. 2013, *JAP*, **114**, 063302
 Stecher, T. P., & Milligan, J. E. 1961, *AJ*, **70**, 296
 Stecher, T. P., & Milligan, J. E. 1962, *ApJ*, **136**, 1
 Tanarro, I., Sanz, M. M., Domingo, C., et al. 1994, *JPhCh*, **98**, 5862
 Watson, J. 1980, *JMoSp*, **80**, 411
 Zinchenko, L., Dubrovich, V., & Henkel, C. 2011, *MNRAS*, **415**, L78